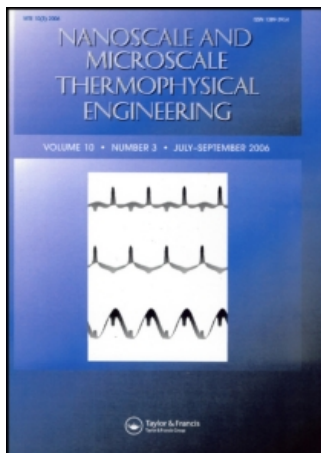


This article was downloaded by:[2007-2008 Seoul National University]  
On: 29 February 2008  
Access Details: [subscription number 769136871]  
Publisher: Taylor & Francis  
Informa Ltd Registered in England and Wales Registered Number: 1072954  
Registered office: Mortimer House, 37-41 Mortimer Street, London W1T 3JH, UK



## Nanoscale and Microscale Thermophysical Engineering

Publication details, including instructions for authors and subscription information:  
<http://www.informaworld.com/smpp/title~content=t713774103>

### On Thermocapillary Propulsion of Microliquid Slug

Ho-Young Kim<sup>a</sup>

<sup>a</sup> School of Mechanical and Aerospace Engineering, Seoul National University, Seoul, Korea

Online Publication Date: 01 July 2007

To cite this Article: Kim, Ho-Young (2007) 'On Thermocapillary Propulsion of Microliquid Slug', *Nanoscale and Microscale Thermophysical Engineering*, 11:3, 351 - 362

To link to this article: DOI: 10.1080/15567260701715495

URL: <http://dx.doi.org/10.1080/15567260701715495>

PLEASE SCROLL DOWN FOR ARTICLE

Full terms and conditions of use: <http://www.informaworld.com/terms-and-conditions-of-access.pdf>

This article maybe used for research, teaching and private study purposes. Any substantial or systematic reproduction, re-distribution, re-selling, loan or sub-licensing, systematic supply or distribution in any form to anyone is expressly forbidden.

The publisher does not give any warranty express or implied or make any representation that the contents will be complete or accurate or up to date. The accuracy of any instructions, formulae and drug doses should be independently verified with primary sources. The publisher shall not be liable for any loss, actions, claims, proceedings, demand or costs or damages whatsoever or howsoever caused arising directly or indirectly in connection with or arising out of the use of this material.

## ON THERMOCAPILLARY PROPULSION OF MICROLIQUID SLUG

**Ho-Young Kim**

*School of Mechanical and Aerospace Engineering, Seoul National University, Seoul, Korea*

*A liquid slug in a microchannel can be propelled by temperature difference between the ends of the slug. This study presents an analytical model to predict the velocity of such slug motion. The models thus far developed only considers very long slugs where the viscous dissipation near the contact line is negligible compared with the bulk dissipation. Therefore, here we develop a novel model to account for the shear stress near the contact line so that it can be applied to slugs of general configuration. It is shown that the bulk dissipation dominates when the slug length is much greater than the channel's hydraulic diameter. However, the wedge dissipation dominates when the slug length is much smaller than the hydraulic diameter. A simple experiment using a mineral oil microslug shows that our theory considering both the wedge and bulk dissipation agrees with the measurement results.*

**KEY WORDS:** thermocapillary, microchannel, contact line, contact angle

### INTRODUCTION

The transport mechanisms of liquid slugs or drops in microscale channels or capillaries are of an immense interest owing to the wide applications of microfluidic technology especially in bioanalytical systems [1–3]. Currently available methods to transport microliquid slugs or drops include the inclination in the gravity field [4], pressure gradients [5], electrowetting [6], electroosmosis [7], chemical modification of wetting properties of the solid surface [8], and thermocapillary process [9]. Among these schemes, our interest in this article lies in the thermocapillary migration of a liquid slug in microchannels.

A liquid drop situated on an open horizontal surface remains stationary until external force is applied. When the thermal gradient is applied along the drop, the drop experiences asymmetrical force because the surface tension coefficient decreases with the temperature. As the force overcomes a threshold value due to the contact angle hysteresis, the drop begins to move. Such a thermocapillary actuation was theoretically studied by Brochard [10] and Ford and Nadim [11] by assuming the drop to be thin (lubrication approximation). The scheme was

This work was supported by the Korea Research Foundation (Grant No. KRF-2005-003-D00033) funded by the Korea government (MOEHRD) through the Basic Research Promotion Fund.

Address correspondence to Professor Ho-Young Kim, Room 302-423, School of Mechanical and Aerospace Engineering, Seoul National University, Seoul 151-744, Korea. E-mail: hyk@snu.ac.kr

experimentally realized by Darhuber et al. [12] using arrays of microheaters. In addition, a continuous liquid stream was shown to be driven by the thermocapillary process on hydrophilic microstripe and its fluid dynamic behavior was theoretically analyzed by Darhuber et al. [13].

On the other hand, the thermocapillary motion of a liquid slug inside microchannels or capillaries has not drawn as active attention as that of a liquid drop on an open surface. Sammarco and Burns [9] showed that a long liquid slug inside a microchannel can be pumped by the thermocapillary process. It was shown that this process could be integrated with the DNA analysis system [14]. The liquid slug used in Sammarco and Burns [9] was very long compared with the microchannel height such that the length-to-height ratio exceeded 100. Therefore, the motion of the slug could be modeled as the Poiseuille flow neglecting the effects of the contact line where the three phases of liquid/solid/gas meet.

However, as today's biochemical micro/nanosystems require an extremely miniscule volume of liquid sample, the slug length cannot always be kept much longer than the channel height. Then the effects of the contact line can no longer be ignored. Thus, a new theoretical model is necessary to predict the thermocapillary migration velocity of a slug of a moderate length. In addition, the aforementioned analytical studies on thermocapillary drop motion adopted a lubrication approximation [10, 11], thus the results are not applicable unless the contact angle is much less than unity (in radian). Therefore, here we theoretically analyze the thermocapillary migration velocity of liquid slugs of general length-to-height ratios and contact angles. In addition, a simple experimental result follows the theoretical considerations.

## THEORY OF THERMOCAPILLARY SLUG PROPULSION

Consider a liquid slug of length  $L$  in a horizontal microchannel as illustrated in Figure 1. The channel has a hydraulic diameter of  $D_h = 4A/P$ , where  $A$  and  $P$  denote the cross-sectional area and the perimeter of the channel, respectively. When the channel is a circular capillary,  $D_h$  is equal to the tube diameter  $D$ . Inside a hydrophilic channel as in the figure, the temperature gradient in the axial direction results in a net force on the slug toward a colder region. Inside a hydrophobic channel, the force direction is reversed.

For a slug with negligible inertia, the driving and resisting forces are balanced. The driving force,  $F_d$ , results from the surface tension acting at the advancing and receding interfaces in the tangential direction. It is written as

$$F_d = P(\sigma_A \cos \theta_A - \sigma_R \cos \theta_R) \quad (1)$$

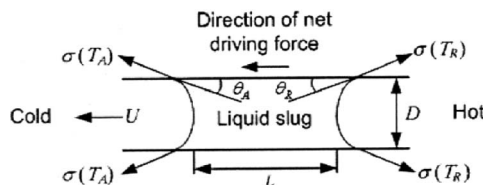


Figure 1. A liquid slug in a hydrophilic capillary under an axial temperature gradient.

where  $\sigma$  and  $\theta$  are the surface tension and the dynamic contact angle, respectively. The subscripts  $A$  and  $R$  denote the advancing and receding interfaces, respectively. In general, both  $\sigma$  and  $\theta$  are functions of the temperature. Especially, the surface tension can be approximated as a linear function of the temperature; i.e.,  $\sigma = a - bT$ , when the temperature range is not too large.

The resisting forces,  $F_r$ , consist of the viscous shear force experienced by the bulk liquid,  $F_b$ ; the shear force in the wedge region near the contact lines,  $F_{w,A}$  and  $F_{w,R}$ ; and the force associated with the motion of fluid molecules between adsorption sites distributed on the solid surface,  $F_l$  [15, 16]. Then we write

$$F_r = F_b + F_{w,A} + F_{w,R} + F_l \tag{2}$$

For a slug moving with the constant velocity  $U$ , the shear force in the bulk region is obtained by the Poiseuille flow solution as  $F_b = \rho f L P U^2 / 8$ , where  $\rho$  is the density and  $f$  is the friction factor defined as  $f = 2D_h \Delta P / \rho L U^2$ ,  $\Delta P$  being the pressure drop. For a fully developed flow through a straight microchannel, it is given that  $f \text{Re} = C$ , where  $\text{Re}$  is the Reynolds number defined as  $\text{Re} = \rho U D_h / \mu$ ,  $\mu$  being the viscosity. The constant  $C$  is determined by the geometric configuration of the channel. Then  $F_b$  is given by

$$F_b = \frac{\mu C P L}{8 D_h} U \tag{3}$$

For a circular tube,  $C = 64$  and consequently  $F_b$  can be written as  $F_b = 8\pi\mu L U$ .

To evaluate the shear force acting near the contact line, we consider the wedge flow as shown in Figure 2. To obtain the shear stress at the wall, the velocity field in the wedge region needs to be solved. For inertia-free flows, the biharmonic equation for the stream function  $\Psi$  is satisfied:  $\nabla^4 \Psi = 0$ . The velocity components are given by  $v_r = -(1/r) \partial \Psi / \partial \theta$  and  $v_\theta = \partial \Psi / \partial r$ . The boundary conditions are such that at  $\theta = 0$ ,  $v_\theta = 0$  and  $v_r = U$ , and at  $\theta = \theta_0$ ,  $v_\theta = 0$  and  $\tau_{r\theta} = 0$ . Here the shear stress  $\tau_{r\theta}$  is given by

$$\tau_{r\theta} = \frac{\mu}{r} \left( \frac{\partial v_r}{\partial \theta} - v_\theta \right) \tag{4}$$

Solving the biharmonic equation with the four boundary conditions, the shear stress at the wall,  $\tau_w = \tau_{r\theta}(\theta = 0)$ , is obtained as

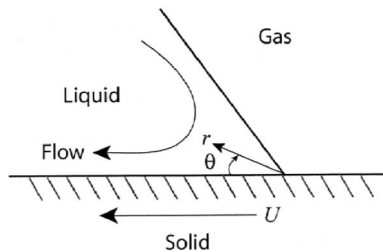


**Figure 2.** The flow field in the wedge near the contact line. Here the reference frame is fixed to the contact line thus the solid is seen to move.

$$\tau_w = \frac{2\mu}{r} U \eta(\theta_0), \quad (5)$$

where  $\eta$  is termed the dissipation factor here and defined as  $\eta(\theta_0) = \sin^2\theta_0/(\theta_0 - \sin\theta_0\cos\theta_0)$ . The shear force in the advancing wedge is given by

$$F_{w,A} = 2\mu PU \eta(\theta_A) \int_{\lambda}^A \frac{dr}{r} \quad (6)$$

where  $\Lambda$  is the radial extension of the wedge. The cutoff length of the molecular scale,  $\lambda$ , has been introduced instead of zero to prevent the integral from tending to infinity [16]. Therefore, the total shear force acting on both the wedge regions becomes

$$F_{w,A} + F_{w,R} = 2\mu PU \left[ \eta(\theta_A) \ln\left(\frac{\Lambda_A}{\lambda_A}\right) + \eta(\theta_R) \ln\left(\frac{\Lambda_R}{\lambda_R}\right) \right] \quad (7)$$

Here we note that our evaluation of the shear force in the wedge region is applicable for any values of the contact angle, contrary to the analysis based on the lubrication approximation [10, 11]. When the lubrication approximation is employed assuming a small contact angle ( $\theta_A \ll 1$ ), the wedge shear force is given by (see Appendix A)

$$F_{w,L} = \frac{3\mu PU}{\theta_A} \ln(\Lambda/\lambda) \quad (8)$$

Comparing Eqs. (7) and (8) reveals that  $\eta(\theta) \approx 3 / 2\theta$  for small  $\theta$ . Figure 3 indeed confirms this prediction, which implies that the current evaluation of the shear force in the wedge given in Eq. (7) is capable of accommodating the limit cases of small contact angles. In a case that  $\theta$  approaches  $180^\circ$ ,  $\eta$  vanishes, meaning no singularity in either the force or the stress at the contact line [17]. The wedge geometry as shown in Figure 2

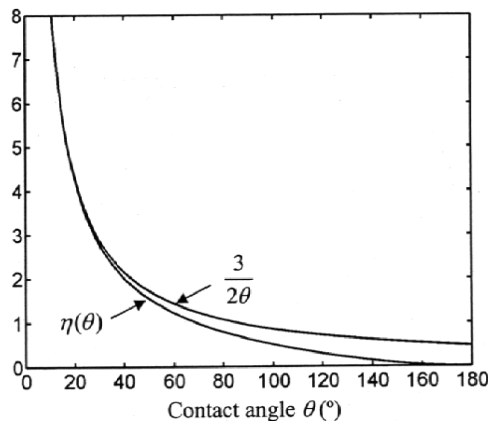


Figure 3. Dissipation factors versus the contact angle.

is invariantly maintained along the entire contact line when the capillary is a circular tube. However, when the capillary is a polygonal channel, the meniscus shape is not defined as simply as in the circular tube. In Appendix B, we discuss the effect of the meniscus shape in the polygonal channel on the wedge shear force.

It is known that the dissipation process related to the molecule's adsorption-desorption motion near the contact line manifests itself as the contact angle hysteresis [18]. That is, the liquid slug does not start to move immediately when an external temperature gradient is applied. The slug begins to move when the driving force exceeds a threshold value associated with the contact angle hysteresis. Therefore,  $F_l$  can be obtained by using the driving force at the moment the slug initiates its motion,  $F_{d,c}$ :

$$F_l = F_{d,c} = P(\sigma_{A,c} \cos \theta_{A,c} - \sigma_{R,c} \cos \theta_{R,c}) \tag{9}$$

where the subscript  $c$  denotes the critical value corresponding to the outset of slug motion.

The force balance of  $F_d = F_r$  yields the steady velocity of a microliquid slug:

$$U = \frac{(\sigma_A \cos \theta_A - \sigma_R \cos \theta_R) - F'_{d,c}}{\mu\{CL/8D_h + 2[\eta(\theta_A) \ln(\Lambda_A/\lambda_A) + \eta(\theta_R) \ln(\Lambda_R/\lambda_R)]\}} \tag{10}$$

where  $F'_{d,c} = F_{d,c}/P$ . If the meniscus shapes of the advancing and receding edges are similar so that

$$\eta(\theta_A) \ln(\Lambda_A/\lambda_A) \approx \eta(\theta_R) \ln(\Lambda_R/\lambda_R) \approx \eta(\theta) \ln(\Lambda/\lambda) \tag{11}$$

where  $\theta$ ,  $\lambda$ , and  $\Lambda$  are the representative values of the corresponding symbols, Eq. (11) can be simplified as

$$U = \frac{(a - bT_A) \cos \theta_A - (a - bT_R) \cos \theta_R - F'_{d,c}}{\mu[CL/8D_h + 4\eta(\theta) \ln(\Lambda/\lambda)]} \tag{12}$$

Equation (12) implies that the steady velocity of a microliquid slug is expressed as a ratio of the driving force to the resisting force.

We note that depending on the ratio of the slug length to the tube hydraulic diameter, the dominant dissipation mechanism may vary. For instance, if a tube diameter is on the order of 100  $\mu\text{m}$ ,  $\Lambda$  can be scaled as the same order. Setting the molecular length scale  $\lambda = 1 \text{ nm}$  and noting that  $\eta$  is of the order 1 for an angle  $0 << \theta << 180^\circ$ , we get  $4\eta \ln(\Lambda/\lambda) \approx 40$ . It is noted that due to a logarithmic nature of this expression, the exact value of  $\Lambda$  and  $\lambda$  do not have a critical influence on the value of  $U$ . Thus, we find that the bulk dissipation is dominant for  $CL/8D_h \gg 40$ . In this case, Eq. (12) reduces to

$$U = \frac{(a - bT_A) \cos \theta_A - (a - bT_R) \cos \theta_R - F'_{d,c}}{\mu CL/8D_h} \tag{13}$$

On the other hand, for a short slug such that  $CL/8D_h \ll 40$ , the wedge dissipation is dominant, thus, the slug velocity is given by:

$$U = \frac{(a - bT_A) \cos \theta_A - (a - bT_R) \cos \theta_R - F'_{d,c}}{4\mu\eta(\theta) \ln(\Lambda/\lambda)} \quad (14)$$

For an intermediate range of the slug length, the full expression of Eq. (12) gives the correct slug velocity. The foregoing expressions can be further simplified in an idealized situation that the contact angles remain the same; i.e.,  $\theta_A = \theta_R = \theta$ . Then Eq. (12) reduces to

$$U = \frac{b(\Delta T - \Delta T_c) \cos \theta}{\mu[CL/8D_h + 4\eta(\theta) \ln(\Lambda/\lambda)]} \quad (15)$$

where  $\Delta T = T_R - T_A$  and  $\Delta T_c$  is the temperature difference at the moment the slug initiates its motion. For a circular tube, Eq. (15) becomes

$$U = \frac{b(\Delta T - \Delta T_c) \cos \theta}{4\mu[L/R + \eta(\theta) \ln(\Lambda/\lambda)]} \quad (16)$$

where  $R$  is the tube radius. So far we have developed a model to predict the steady velocity of a microliquid slug of a general configuration driven by the thermocapillarity. The following section describes a simple experiment that illustrates the importance of considering both the wedge and bulk dissipation in modeling the slug velocity.

## SIMPLE EXPERIMENT

For a long slug where the wedge dissipation is negligible as compared with the bulk dissipation, Sammarco and Burns [9] performed experiments to verify Eq. (13). Therefore, the major interest in the current experiment is to illustrate the influence of the wedge dissipation on the migration velocity of a relatively short slug. We use a circular capillary tube with inner diameter 700  $\mu\text{m}$  made of borosilicate glass. To induce the temperature difference between the slug ends, the tube is wrapped with a nichrome heater near one of the tube ends. To the other end, an aluminum fin is attached and then immersed in ice water for cooling. Four thermocouples are attached to the tube for temperature measurement. As a slug liquid, mineral oil (Aldrich Chemical, Milwaukee, Wisconsin) is used. For the mineral oil,  $\mu = 0.026 \text{ Pa}\cdot\text{s}$ ,  $a = 0.0471 \text{ N/m}$ , and  $b = 2.21 \times 10^{-4} \text{ N/m}/^\circ\text{C}$ . The motion of the slug is recorded by a CCD camera whose images are captured and analyzed by a digital computer.

Since one end of the capillary tube is heated, temperature monotonically drops towards the other end. The measured temperature profile as shown in Figure 4 indicates nonlinear decrease of temperature along the tube axis. This temperature distribution,  $T(x)$ , can be predicted by modeling the tube as a fin governed by the following energy balance equation:

$$\frac{d^2\psi}{dx^2} - m^2\psi = 0 \quad (17)$$

where  $\psi$  is the difference of tube temperature  $T$  and the end temperature  $T_\infty$ ,  $\psi = T - T_\infty$ ,  $x$  is the distance measured from the hottest thermocouple, and  $m^2$  is given by the

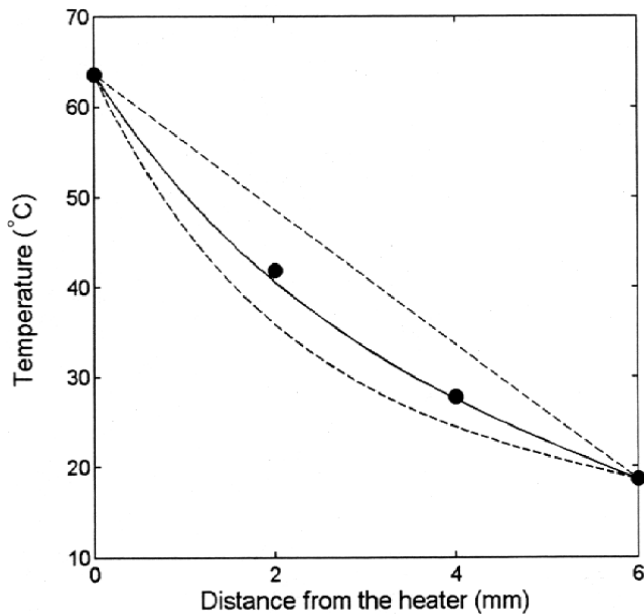


**Figure 4.** Temperature distribution along the capillary tube. The solid circles denote measurement results. The dashed straight line is for a perfectly insulated capillary tube. The solid line is the solution of Eq. (17) with the heat transfer coefficient being a half that of a horizontal cylinder. The dashed curve is when the heat transfer coefficient of an uncovered horizontal cylinder is used in the fin analysis.

natural convection heat transfer coefficient  $h$ , the effective outer periphery  $L$ , the thermal conductivity of the glass tube  $k$ , and the cross-sectional area of the tube  $A_c$ , as  $m^2 = hL/kA_c$ . Since the capillary tube lies on an insulating surface, we take the effective periphery  $L$  as half the outer circumference and  $h$  as half the heat transfer coefficient for a heated horizontal cylinder. Then the predicted temperature profile and the measurement results show good agreement.

Due to the nonlinear temperature profile, the values of  $(T_R - T_A)$  were different as the slug moved along the tube. We used a mineral oil slug of 2.0 mm in length. As the slug moved along the tube, the temperature difference between the slug ends ranged between 14.2 and 17°C. Now we check whether the slug inertia is negligibly small in this experiment. The inertia of the slug is scaled as  $\rho VU^2/L$ , where  $\rho$  and  $V$  denote the density and the volume of the slug, respectively. The viscous shear force in the bulk region is scaled as  $\mu UPL/R$ . The ratio of the inertia to the shear force is less than  $4 \times 10^{-4}$  using the maximum velocity of Figure 5 even without considering the wedge shear force. Thus, the inertia of the slug is indeed negligibly small and our foregoing analysis can be applied.

Figures 5 and 6 show the experimental image of the slug and the velocity measurement results compared with predictions by different theoretical considerations, respectively. Since the advancing and receding angles of the slug are very similar as confirmed by Figure 6 ( $\theta \approx 45^\circ$ ), we employ Eq. (16) for comparison with the experimental results. We plot three different velocity predictions based on Eq. (16) to evaluate the effects of each dissipation mechanisms. Although the velocity values may

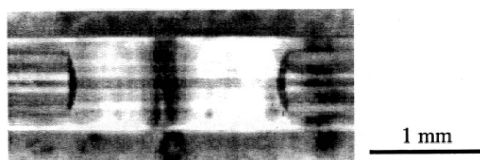


**Figure 5.** Image of a mineral oil slug in a capillary. Shown as dark vertical lines behind the tube are the thermocouples attached to the tube

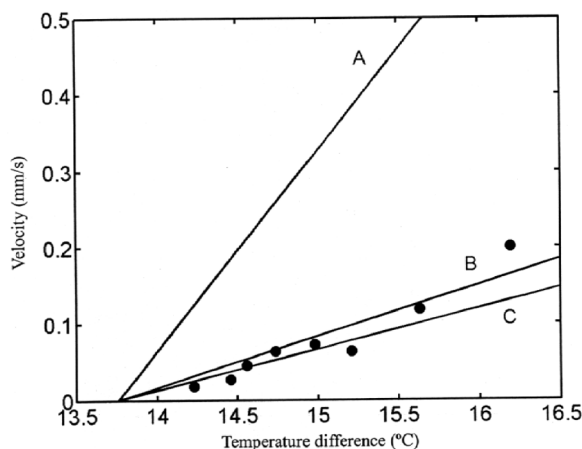


**Figure 6.** Comparison of the results of the experiments (solid circles) and those of the analysis (lines). Lines A and B correspond to the velocity when the wedge dissipation and the bulk dissipation are neglected, respectively. Line C is from Eq. (16). In plotting the theoretical velocity, we used  $\Lambda = R = 350 \mu\text{m}$ ,  $\lambda = 1 \text{ nm}$ , and  $\Delta T_c = 13.8^\circ\text{C}$ .

vary depending on  $\Delta T_c$ , which is hard to control in a repeatable manner, it is the slope of the curve that directly indicates the effects of the viscous stresses. Under our experimental condition of  $L/R = 5.7$ , the ratio of the bulk stress to the wedge stress,  $(L/R)/[\eta \ln(\Lambda/\lambda)]$  (see the denominator of Eq. (16)), amounts to be only 0.26. Therefore, when the wedge shear stress is neglected as in line A in Figure 6, the theoretical line's slope highly overestimates that of the experimental results. On the other hand, line B, which ignores the bulk dissipation, is close to line C obtained directly from Eq. (16) considering both the bulk and wedge stresses. Both lines B and C (especially their slopes) agree favorably with the experimental results. This result clearly shows the importance of considering the wedge dissipation in modeling the short slug's movement.

We recall that the evaluation of the wedge dissipation involves the order-of-magnitude estimations of  $\lambda$  and  $\Lambda$ . To investigate the sensitivity of the theoretical results to the variation of  $\lambda$  and  $\Lambda$ , we plotted the velocity values corresponding to the current experimental conditions for different values of  $\Lambda/\lambda$  in Figure 7. The range considered in the plot corresponds to the variation of the cutoff length over two orders when  $\Lambda$  is fixed. Such a great degree of variation results in the change of the predicted velocity only within  $\pm 20\%$ . This shows that the approximate nature of the evaluation for the wedge dissipation does not critically affect the analysis outcomes.

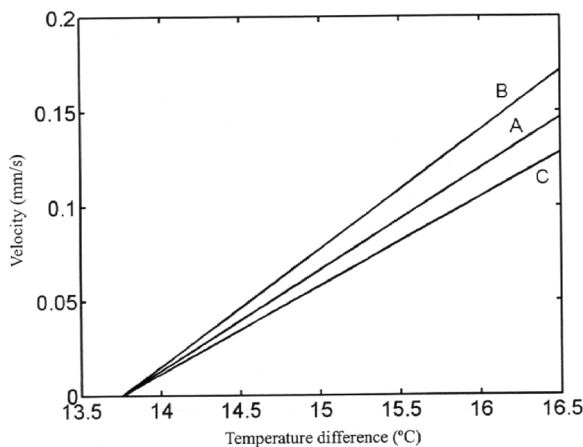


**Figure 7.** Sensitivity of the theoretical results to the variation of  $\lambda$  and  $\Lambda$ . Line A is the same as line C of Fig. 6. Lines B and C correspond to  $\lambda = 10$  nm and 0.1 nm, respectively with  $\Lambda = 350$   $\mu$ m fixed. If  $\lambda$  is fixed at 1 nm, lines B and C correspond to  $\Lambda = 35$   $\mu$ m and 3.5 mm, respectively.

## SUMMARY

This study considers the thermocapillary migration velocity of viscous slugs in a capillary tube. We newly develop a theoretical model to predict the slug velocity using the balance between the driving force (surface tension force due to temperature difference) and the resisting force (viscous dissipation). We note that the viscous dissipation consists of the bulk dissipation occurring in the central region of the slug and the wedge dissipation near the contact lines. Our model is capable of evaluating the viscous dissipation in the wedge regions of slugs having relatively large contact angles where the lubrication approximation is invalid. The bulk dissipation dominates when the slug length is much larger than the channel's hydraulic diameter but the wedge dissipation dominates when the slug length is much smaller than the hydraulic diameter. Through a simple experiment using a mineral oil slug in a circular capillary tube, we find that our theoretical velocity prediction considering both the wedge and bulk dissipation agrees well with the measurement results.

## REFERENCES

1. D.L. Polla, A.G. Erdman, W.P. Robbins, D.T. Markus, J. Diaz-Diaz, R. Rizq, Y. Nam, H.T. Brickner, A. Wang, and P. Krulevitch, *Microdevices in Medicine, Annual Review of Biomedical Engineering*, vol. 2, pp. 551–576, 2000.
2. D.R. Meldrum and M.R. Holl, *Microscale Bioanalytical Systems, Science*, vol. 297, pp. 1197–1198, 2002.
3. H.A. Stone, A.D. Stroock, and A. Ajdari, *Engineering Flows in Small Devices: Microfluidics Toward a Lab-on-a-Chip, Annual Review of Fluid Mechanics*, vol. 36, pp. 381–411, 2004.
4. J. Bico and D. Quere, *Falling Slugs, Journal of Colloid and Interface Science*, vol. 243, pp. 262–264, 2001.
5. J. Pfahler, J. Harley, H. Bau, and J. Zemel, *Liquid Transport in Micron and Submicron Channels, Sensors and Actuators A*, vol. 21–23, pp. 431–434, 1990.

6. J. Lee and C.-J. Kim, Surface Tension Driven Microactuation Based on Continuous Electrowetting (CEW), *Journal of Microelectromechanical Systems*, vol. 198, pp. 171–180, 2000.
7. S.F. Bart, L.S. Tavrow, M. Mehregany, and J.H. Lang, Microfabricated Electrohydrodynamic Pumps, *Sensors and Actuators A*, vol. 21–23, pp. 193–197, 1990.
8. M.K. Chaudhury and G.M. Whitesides, How to Make Water Run Uphill, *Science*, vol. 256, pp. 1539–1541, 1992.
9. T.S. Sammarco and M.A. Burns, Thermocapillary Pumping of Discrete Drops in Microfabricated Analysis Devices, *AIChE Journal*, vol. 45, pp. 350–366, 1999.
10. F. Brochard, Motions of Droplets on Solid Surfaces Induced by Chemical or Thermal Gradients, *Langmuir*, vol. 5, pp. 432–438, 1989.
11. M.L. Ford and A. Nadim, Thermocapillary Migration of an Attached Drop on a Solid Surface, *Physics of Fluids*, vol. 6, pp. 3183–3185, 1994.
12. A.A. Darhuber, J.P. Valentino, S.M. Troian, and S. Wagner, Thermocapillary Actuation of Droplets on Chemically Patterned Surfaces by Programmable Microheater Arrays, *Journal of Microelectromechanical Systems*, vol. 12, pp. 873–879, 2003.
13. A.A. Darhuber, J.M. Davis, S.M. Troian, and W.W. Reisner, Thermocapillary Actuation of Liquid Flow on Chemically Patterned Surfaces, *Physics of Fluids*, vol. 15, pp. 1295–1304, 2003.
14. M.A. Burns, et al. Microfabricated Structures for Integrated DNA Analysis, *Proceedings of the National Academy of Sciences USA*, vol. 93, pp. 5556–5561, 1996.
15. P.G. de Gennes, Wetting: Statics and Dynamics, *Reviews of Modern Physics*, vol. 57, pp. 827–863, 1985.
16. H.-Y. Kim, H.J. Lee, and B.H. Kang, Sliding of Liquid Drops Down an Inclined Solid Surface, *Journal of Colloid and Interface Science*, vol. 247, pp. 372–380, 2002.
17. L. Mahadevan and Y. Pomeau, Rolling Droplets, *Physics of Fluids*, vol. 11, pp. 2449–2453, 1999.
18. T.D. Blake and J.M. Haynes, Kinetics of Liquid/Liquid Displacement, *Journal of Colloid and Interface Science*, vol. 30, pp. 421–423, 1969.
19. H. Wong, S. Morris, and C.J. Radke, Three-Dimensional Menisci in Polygonal Capillaries, *Journal of Colloid and Interface Science*, vol. 148, pp. 317–336, 1992.
20. E. Kim and G.M. Whitesides, Imbibition and Flow of Wetting Liquids in Noncircular Capillaries, *Journal of Physical Chemistry B*, vol. 101, pp. 855–863, 1997.

## APPENDIX A LUBRICATION APPROXIMATION FOR WEDGE SHEAR FORCE

Here we obtain the shear force at the wedge near the contact line when the contact angle is very small, thus, the lubrication approximation can be used. For a thin wedge as shown in Figure 8, the flow is nearly parallel to the solid surface and its motion is governed by the following equation:

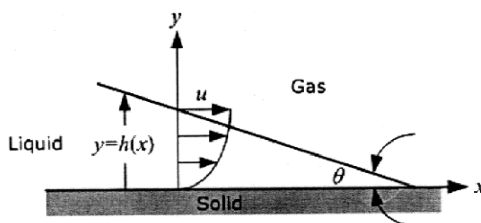


Figure 8. Flow profile in a thin wedge for which the lubrication approximation is made.

$$\frac{dp}{dx} = \mu \frac{\partial^2 u}{\partial y^2} \quad (\text{A1})$$

where  $p$  is the pressure and  $u$  is the  $x$ -directional velocity. The boundary conditions are such that  $u = 0$  at the solid surface  $y = 0$ , and  $\partial u / \partial y = 0$  at the liquid/gas interface  $y = h(x)$ . Solving Eq. (A1) and equating the resultant average flow velocity to  $U$ , we find

$$u = \frac{3U}{h^2} \left( hy - \frac{y^2}{2} \right) \quad (\text{A2})$$

Then the wall shear stress becomes  $\tau_w = 3\mu U/x\theta$ , where we used  $h = x\theta$  for small  $\theta$ . Integrating this over the wedge area yields the shear force:

$$F_w = P \int_{\lambda}^{\Lambda} \frac{3\mu U}{x\theta} dx \quad (\text{A3})$$

which becomes equal to Eq. (8).

## APPENDIX B MENISCUS AND WEDGE SHEAR FORCE IN POLYGONAL CHANNEL

The shear force experienced in the wedge region was evaluated based on the geometry as shown in Figure 2. Although this geometry is valid when the capillary tube is circular, the meniscus shape is rather complicated when the capillary is a polygonal channel. Meniscus shapes in polygonal capillaries were theoretically calculated in [19] and experimentally visualized in [20]. The images of menisci in [20] show negligible wicking into corners when the contact angle is greater than about  $45^\circ$ . In this case, the formulation for the wedge dissipation as used for the circular capillary is valid. On the other hand, the imbibition was well pronounced in the corners when the contact angle was lower than  $45^\circ$ , as shown in Figure B1. Then the wedge dissipation consists of that occurring in the central part and that in the shoulders, as indicated in Figure B1. The central wedge dissipation is obtained by the identical formulation as in the circular capillary. The shear stress in a shoulder can be scaled as  $\tau_{w,s} \sim \mu U/\delta$ , where  $\delta$  is the thickness of the shoulder at a location  $\zeta$  thus given by  $\delta \sim \zeta\theta$ . The shear force in the shoulder is obtained by integrating the shear stress over the shoulder area of length  $\tilde{\zeta}$

$$F_{w,s} \sim \int_0^{\tilde{\zeta}} \tau_{w,s} \delta d\zeta \sim \mu U \tilde{\zeta} \quad (\text{B1})$$

It is interesting to note that when the meniscus imbibes in the corners of polygonal capillaries, the shear force does not diverge as contrary to that at the normal contact line on a plane. We compare the magnitude of this shoulder shear stress with the usual wedge shear stress by taking the ratio

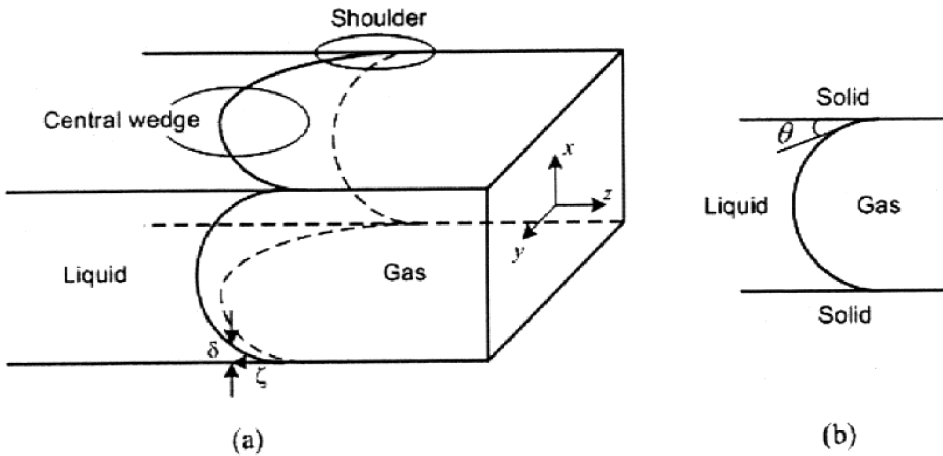


**Figure B1.** (a) Menisci in the rectangular capillary. (b) Meniscus intersecting with the  $y$ - $z$  or  $x$ - $z$  planes.

$$\alpha = \frac{F_{w,s}}{F_w} \sim \frac{\zeta}{P\eta \ln(\Lambda/\lambda)} \quad (\text{B2})$$

When the shoulder is relatively short so that  $\alpha \ll 1$ , the effect of the corner imbibition on the wedge shear stress is negligible. If the shoulder is long enough to make  $\alpha \sim 1$ , then the corner imbibition should be taken into account in evaluating the wedge shear stress. Based on the images of Kim and Whitesides [20], when the contact angle is above about  $40^\circ$ , the shoulder is short enough to neglect  $\alpha$ . The images of Kim and Whitesides [20] further show that as the contact angle decreases, the imbibition length  $\zeta$  increases, elevating the possibility that  $\alpha$  may increase. However, it should be noted that  $\eta$  also increases sharply as the contact angle decreases. Thus the increase of  $\zeta$  does not necessarily guarantee the increase of  $\alpha$ . The detailed theory to compute  $\alpha$  for a low contact angle is beyond the scope of the present study.